
IPSeg: Image Posterior Mitigates Semantic Drift in Class-Incremental Segmentation

Xiao Yu^{1,2,*} Yan Fang^{1,2,*} Yao Zhao^{1,2} Yunchao Wei^{1,2,✉}

¹ Institute of Information Science, Beijing Jiaotong University ² Visual Intelligence + X International Joint Laboratory

*equal contributors ✉corresponding author

wychao1987@gmail.com

Abstract

Class incremental learning aims to enable models to learn from sequential, non-stationary data streams across different tasks without catastrophic forgetting. In class incremental semantic segmentation (CISS), the semantic content of image pixels evolves over incremental phases, known as **semantic drift**. In this work, we identify two critical challenges in CISS that contribute to semantic drift and degrade performance. First, we highlight the issue of separate optimization, where different parts of the model are optimized in distinct incremental stages, leading to misaligned probability scales. Second, we identify noisy semantics arising from inappropriate pseudo-labeling, which results in sub-optimal results. To address these challenges, we propose a novel and effective approach, Image Posterior and Semantics Decoupling for Segmentation (IPSeg). IPSeg introduces two key mechanisms: (1) leveraging image posterior probabilities to align optimization across stages and mitigate the effects of separate optimization, and (2) employing semantics decoupling to handle noisy semantics and tailor learning strategies for different semantics. Extensive experiments on the Pascal VOC 2012 and ADE20K datasets demonstrate that IPSeg achieves superior performance compared to state-of-the-art methods, particularly in challenging long-term incremental scenarios. Our code is now available at <https://github.com/YanFangCS/IPSeg>.

1. Introduction

Deep learning methods have achieved significant success in vision (Qu et al., 2021) and language (Ke & Liu, 2022) tasks with fixed or stationary data distributions. However, real-world scenarios are characterized by dynamic and non-stationary data distributions, posing the challenge of *catastrophic forgetting* (McCloskey & Cohen, 1989; McClelland

et al., 1995). Incremental learning, a.k.a. continual learning or lifelong learning (Silver et al., 2013), has been proposed to enable models to adapt to new data distributions without forgetting previous knowledge (Kudithipudi et al., 2022). Within this domain, Class Incremental Learning (CIL) methods (Serra et al., 2018; Li & Hoiem, 2017; Rebuffi et al., 2017; Mai et al., 2022; Wang et al., 2024a) have shown great potential in learning new classes from incoming data, particularly for classification tasks (De Lange et al., 2021).

Class Incremental Semantic Segmentation (CISS) extends the principles of CIL to pixel-wise tasks. In addition to catastrophic forgetting, CISS encounters an even more critical challenge: *semantic drift* (Yuan & Zhao, 2023) or *background shift* (Cermelli et al., 2020), which describes the incremental change in the semantic meaning of pixel labels. Several studies (Douillard et al., 2021; Cha et al., 2021; Zhang et al., 2022b; 2023) attribute *semantic drift* to the evolving semantic content of the background across incremental stages. Subsequent works (Cermelli et al., 2020; Douillard et al., 2021) early pioneer this investigation using knowledge distillation and pseudo-labeling. More recent works (Cha et al., 2021; Zhang et al., 2022b; 2023) further use saliency maps and segment proposals to differentiate between the foreground and background pixels. These works introduce naive and inappropriate pseudo-labeling, ignoring decoupling the learning of these semantics, leaving *noisy semantics* remains a critical challenge to be solved.

In this paper, we delve into *semantic drift* challenge and identify an additional but more essential issue, *separate optimization*. *Separate optimization* refers to the learning manner within CISS methods that independently and sequentially update the task heads for each target class set and freeze previous task heads to prevent catastrophic forgetting. This leads to a scenario in which different task heads trained in different stages always have misaligned probability scales, especially on similar-looking classes. It finally results in error classification and magnifying semantic drift. Figure 1(a) directly presents the impact of *separate optimization*, where the SSUL-M model mistakenly classifies a horse as a “cow”

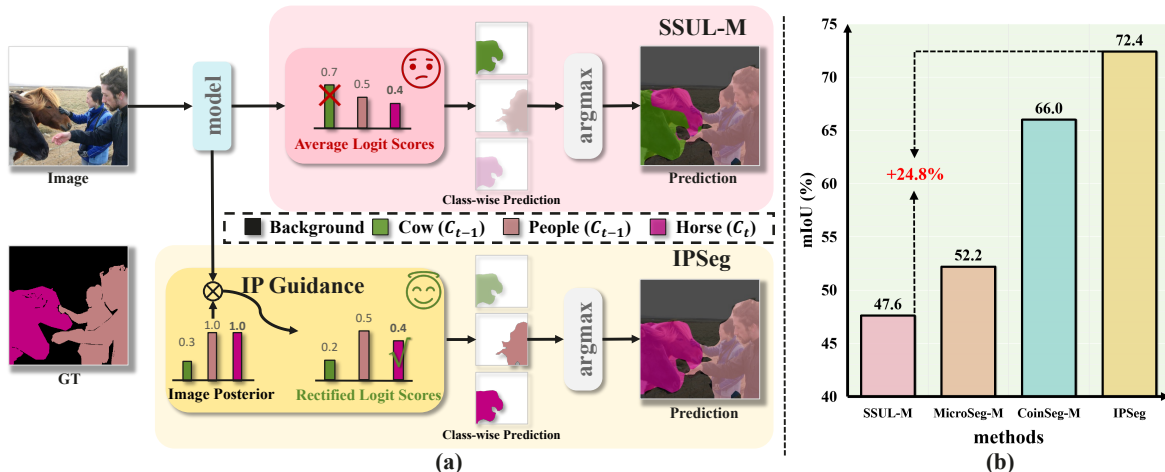


Figure 1: (a) Due to the existence of *separate optimization*, the previous method SSUL-M misclassifies a “horse” as a “cow” with higher logit scores when learning “horse” following “cow”. While our IPSeg leverages image posterior (IP) guidance to produce accurate predictions on these two similar-look classes. The “logit scores” refer to pixel-wise prediction, and the image posterior refers to our introduced image-wise prediction. The logit numbers are used for better illustration. (b) The quantitative performance comparison with state-of-the-art methods under the long-term incremental challenge (VOC 2-2).

class with a higher logit score when separately training the corresponding task heads. Under the combined impacts of *separate optimization* and *noisy semantics*, the previous efforts are still short of effectively addressing the *semantic drift* challenge.

Motivated by our observations and analyses, we introduce **Image Posterior** and **Semantics Decoupling** for Class-Incremental Semantic Segmentation (IPSeg) to address the aforementioned challenges. We propose **image posterior guidance** to mitigate *separate optimization* by rectifying the misaligned pixel-wise predictions using image-wise predictions. As illustrated in Figure 1(a), IPSeg correctly predicts “horse” with the assistance of image posterior guidance. Furthermore, we propose **permanent-temporary semantics decoupling** to decouple *noisy semantics* into two groups, one characterized by simple and stable semantics, and the other by complex and dynamic semantics. We also introduce separate learning strategies for better decoupling.

Extensive experimental results on two popular benchmarks, Pascal VOC 2012 and ADE20K, demonstrate the effectiveness and robustness of IPSeg. Our method consistently outperforms the state-of-the-art methods across various incremental scenarios, particularly in long-term challenges as gaining **24.8%** improvement in VOC 2-2 task.

2. Related Work

Class Incremental Learning (CIL) Class-incremental learning is a method that continuously acquires knowledge in the order of classes, aiming to address catastrophic forgetting (McCloskey & Cohen, 1989). Existing work (Wang

et al., 2024b) broadly categorizes these approaches into three main types. Replay-based methods involve storing data or features of old classes or generating data that includes old classes. They can be further divided into Experience Replay (Rebuffi et al., 2017; Bang et al., 2021), Generative Replay (Liu et al., 2020; Shin et al., 2017), and Feature Replay (Belouadah & Popescu, 2019). Regularization-based methods focus on designing loss functions that incorporate second-order penalties based on the contribution of parameters to different tasks (Kirkpatrick et al., 2017; Jung et al., 2020). They also rely on knowledge distillation, using the model from the previous phase as a teacher to constrain current model (Li & Hoiem, 2017; Rebuffi et al., 2017; Douillard et al., 2020; Buzzega et al., 2020). Architecture-based methods dynamically adjust model parameters based on new data, including assigning specific parameters for different data (Gurbuz & Dovrolis, 2022; Serra et al., 2018) and breaking down model parameters into task-specific or shared parts (Douillard et al., 2022).

Class Incremental Semantic Segmentation (CISS)

CISS is similar to class incremental learning (CIL) but extends the task to pixel-level predictions (Phan et al., 2022; Camuffo & Milani, 2023; Zhang et al., 2022a; Xiao et al., 2023). MiB (Cermelli et al., 2020) first introduces the concept of semantic shift unique to CISS, employing distillation strategies to mitigate this issue. PLOP (Douillard et al., 2021) utilizes pseudo-labeling techniques for incremental segmentation to address background shift, while SSUL (Cha et al., 2021) further incorporates salient information, introducing the concept of “unknown classes” into each learning phase and using a memory pool to store old data to pre-

vent catastrophic forgetting. RECALL (Maracani et al., 2021) and DiffusePast (Chen et al., 2023) extend traditional replay methods by incorporating synthetic samples of previous classes generated using Diffusion (Ho et al., 2020) or GAN (Goodfellow et al., 2020) models. MicroSeg (Zhang et al., 2022b) employs a proposal generator to simulate unseen classes. CoinSeg (Zhang et al., 2023) highlights differences within and between classes, designing a contrastive loss to adjust the feature distribution of classes. PFCSS (Lin et al., 2023) emphasizes the preemptive learning of future knowledge to enhance the model’s discrimination ability between new and old classes.

3. Method

In this section, we begin by presenting the necessary notation and definition of the problem, followed by our analysis of *semantic drift* in Section 3.1. Next, we introduce our proposed method, IPSeg, with detailed designs including image posterior and semantics decoupling in Section 3.3 and Section 3.4.

3.1. Preliminary

Notation and problem formulation Following previous works (Cha et al., 2021; Zhang et al., 2022b; 2023), in CISS, a model needs to learn the target classes $\mathcal{C}_{1:T}$ from a series of incremental tasks as $t = 1, 2, 3, \dots, T$. For task t , the model learns from a unique training dataset \mathcal{D}_t which consists of training data and ground truth pairs $\mathcal{D}_t = \{(x_i^t, y_i^t)\}_{i=1}^{|\mathcal{D}_t|}$. Here i denotes the sample index, t for the task index, and $|\mathcal{D}_t|$ for the training dataset scale. $x_{i,j}^t$ and $y_{i,j}^t$ denote the j -th pixels and the annotation in the image x_i^t . In each incremental phase t , the model can only access the class set $\mathcal{C}_t \cup c_b$ where \mathcal{C}_t denotes the class set of current task t and c_b for background class.

To prevent catastrophic forgetting, architecture-based methods allocate and optimize distinct sets of parameters for each class, instead of directly updating the whole model f_t . Typically, f_t is composed of a frozen backbone h_θ and a series of learnable task heads $\phi_{1:t}$, with one task head corresponding to a specific task. In task t , only the new task head ϕ_t is set to be optimized. In inference, the prediction for the j -th pixel in image x_i can be obtained by:

$$\hat{y}_{i,j} = f_t(x_{i,j}) = \arg \max_{c \in \mathcal{C}_{1:T}} \phi_{1:T}^c(h_\theta(x_{i,j})). \quad (1)$$

Where $\phi_{1:T}^c(\cdot)$ denotes the C -dimension outputs. Additionally, we introduce the image-level labels \mathcal{Y}_i of the image x_i , a memory buffer \mathcal{M} , and an extra image classification head ψ in our implementation. A comprehensive list and explanation of symbols can be found in the appendix.

Semantic Drift Previous work (Kirkpatrick et al., 2017) mainly attributes the *semantic drift* to *noisy semantics* within

the background class c_b . They attempt to mitigate this challenge by decoupling the class c_b into subclasses c'_b and c_u , where c'_b denotes the pure background and c_u denotes the unknown class. The most advanced methods (Zhang et al., 2022b; Cha et al., 2021) further decouple the unknown classes c_u into past seen classes $\mathcal{C}_{1:t-1}$ and dummy unknown class c'_u using pseudo labeling. However, *semantic drift* remains unresolved as the decoupled classes are still evolving across incremental phases while the coupled training strategy is not able to cope with noisy pseudo labels.

Additionally, another essential challenge, *separate optimization* inherent within incremental learning also contributes to *semantic drift* but attracts little attention. Recent work (Kim et al., 2024) finds a similar phenomenon that freezing parameters from the old stage can preserve the model’s prior knowledge but introduces error propagation and confusion between similar classes. In architecture-based methods, the task head ϕ_t is exclusively trained by supervision from the current classes and will be frozen to resist catastrophic forgetting in the following incremental phases. In the following task $t_1, t_1 > t$, ϕ_t may predict high scores on objects from other appearance-similar classes, without any penalty and optimization. In this incremental learning manner, task heads trained in different stages always have misaligned probability scales, and generate error predictions, especially on similar classes. This *separate optimization* manner ultimately causes the incremental models to misclassify some categories and makes *semantic drift* more difficult to thoroughly address. In the appendix, some cases can be found to help understand this challenge.

3.2. Overview

As illustrated in Figure 2, we propose Image Posterior and Semantics Decoupling for Class-incremental Semantic Segmentation (IPSeg) to mitigate *semantic drift* through two main strategies: image posterior guidance and permanent-temporary semantics decoupling. In Section 3.3, we describe how the IPSeg model uses image posterior guidance to mitigate *separate optimization*. To address *noisy semantics*, IPSeg employs branches with different learning cycles to decouple the learning of noisy semantics. Detailed explanations of this approach are provided in Section 3.4.

3.3. Image Posterior Guidance

As previously discussed, the *separate optimization* leads to misaligned probability scales across different incremental task heads and error predictions. We propose leveraging the image-level posterior as the global guidance to correct the probability distributions of different task heads. The rationale for using the image posterior probabilities is based on the following fact:

Fact: For any image, if its image-level class domain is \mathcal{C}_1

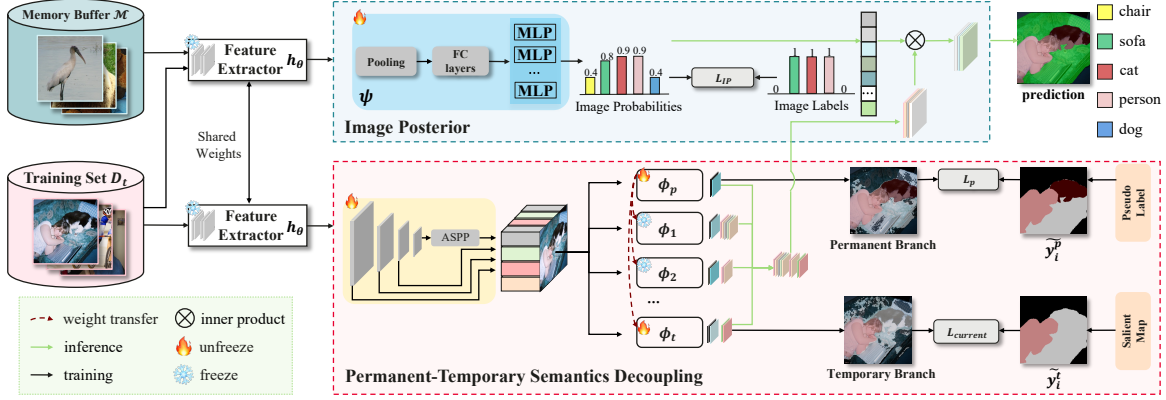


Figure 2: Overall architecture of our proposed IPSeg, mainly composed of image posterior and permanent-temporary semantics decoupling two parts. In the latter part, ϕ_p denotes the permanent learning branch and $\phi_1, \phi_2, \dots, \phi_t$ for temporary ones. The black solid lines are used to indicate the data flow in training and the green ones are for inference.

and its pixel-level class domain is \mathcal{C}_P , the class domains \mathcal{C}_I and \mathcal{C}_P are the same, i.e., $\mathcal{C}_I = \mathcal{C}_P$.

Inspired by this fact, we propose to use an extra image posterior branch ψ to predict image classification labels and train it in an incremental learning manner. As illustrated in Figure 2, ψ is composed of Pooling, Fully connected (FC) layers, and Multi-Layer Perceptrons (with one MLP per step) with the input dimension of 4096 and the output dimension of $|\mathcal{C}_{1:T}|$, where the FC layers serve as shared intermediate feature processors, and the MLPs serve as incremental classification heads for incremental classes.

In task t ($t > 1$), the model can only access data x_i^m from the memory buffer \mathcal{M} and x_i^t from the current training dataset \mathcal{D}_t . Previous works (Cha et al., 2021; Zhang et al., 2023) put x_i^m into the training phase to revisit and reinforce prior knowledge of segmentation by simply rehearsal. IPSeg further takes advantage of the rich class distribution knowledge in x_i^m to train and enhance the image posterior branch.

In IPSeg, the mixed data samples $x_i^{m,t}$ from \mathcal{M} and \mathcal{D}_t are processed by the network backbone h_θ into the image feature $h_\theta(x_i^{m,t})$, and further processed by image posterior branch ψ into the image classification prediction $\hat{\mathcal{Y}}_i^{m,t}$. The objective function for training ψ is:

$$\begin{aligned} \mathcal{L}_{IP} &= \mathcal{L}_{BCE}(\hat{\mathcal{Y}}_i^{m,t}, \tilde{\mathcal{Y}}_i^{m,t}) = \mathcal{L}_{BCE}(\psi(h_\theta(x_i^{m,t})), \tilde{\mathcal{Y}}_i^{m,t}), \\ \tilde{\mathcal{Y}}_i^{m,t} &= \mathcal{Y}_i^{m,t} \cup \tilde{\mathcal{Y}}_{\phi_{1:t-1}(h_\theta(x_i^{m,t}))}. \end{aligned} \quad (2)$$

Where image classification label $\tilde{\mathcal{Y}}_i^{m,t}$ consists of two parts, the ground truth label $\mathcal{Y}_i^{m,t}$ of the data $x_i^{m,t}$ and pseudo label $\tilde{\mathcal{Y}}_{\phi_{1:t-1}(h_\theta(x_i^{m,t}))}$ on past seen classes $\mathcal{C}_{1:t-1}$. Instead of relying solely on the label $\mathcal{Y}_i^{m,t}$, we use the image-level pseudo labels from previous task heads prediction to enhance the model’s discriminative ability on prior classes.

During inference, the image posterior branch predicts poste-

rior probabilities on all classes $\mathcal{C}_{1:T}$. For a testing image x_i , the final pixel-wise scores are computed by element-wise multiplication between the image posterior probabilities from ψ and the pixel-wise probabilities from $\phi_{0:T}$:

$$p_i = \underbrace{\text{Concat}(\alpha_{BC}, \sigma(\psi(h_\theta(x_i))))}_{\text{Image Posterior Probability}} \cdot \underbrace{\sigma(\phi_{0:T}(h_\theta(x_i)))}_{\text{Pixel-wise Probability}}. \quad (3)$$

Where $\sigma(\cdot)$ denotes the Sigmoid function. The hyperparameter α_{BC} is used to compensate for the lack of background posterior probability, with the default value $\alpha_{BC} = 0.9$. The result p_i is the rectified pixel-wise prediction with a shape of $[C, HW]$, and $p_{i,j}^c$ is prediction of the j -th pixel on class c . The prediction of the j -th pixel can be written as:

$$\hat{y}_{i,j} = \arg \max_{c \in \mathcal{C}_{1:t}} p_{i,j}^c. \quad (4)$$

3.4. Permanent-Temporary Semantics Decoupling

To further address *semantic drift* caused by the coupled learning of complex and noisy pseudo labels c_b and c_u along with incomplete yet accurate label \mathcal{C}_t , we propose a decoupling strategy that segregates the learning process for different semantics. Here is our empirical observation:

Observation: Given an image in incremental task t , the semantic contents of it can be divided into four parts: past classes $\mathcal{C}_{1:t-1}$, target classes \mathcal{C}_t , unknown foreground c'_u and pure background c'_b .

Based on this observation, we first introduce dummy label $c_f = \mathcal{C}_{1:t-1} \cup c'_u$ to represent the foreground regions that encompass both past seen classes and unknown classes, which are not the primary targets in the current task. Subsequently, we decouple the regions of a training image into two sets: $\mathcal{C}_t \cup c_f$ and $c'_b \cup c'_u$. The former set $\mathcal{C}_t \cup c_f$ are current target classes and other foreground objects, which are tem-

porary concepts belonging to specific incremental steps, and change drastically as the incremental steps progress. In contrast, $c'_b \cup c'_u$ are pseudo labels representing pure background and unknown objects, which are permanent concepts, exist across the whole incremental steps and maintain stable (c'_b remains fixed, c'_u shrinks but does not disappear).

The learning of these two sets is also decoupled. The current task head ϕ_t serves as the temporary branch to learn the semantics $\mathcal{C}_t \cup c_f$ existing in the current incremental phase. Besides, we introduce a permanent branch ϕ_p to learn the permanent dummy semantics c'_b and c'_u . ϕ_p has the same network architecture as ϕ_t . They are composed of three 3x3 convolution layers and several upsampling layers. It's worth noting that ϕ_p and ϕ_t have different learning cycles as illustrated in Figure 2. The permanent branch ϕ_p is trained and optimized across all incremental phases to distinguish unknown objects and the background. While temporary branch ϕ_t ($t = 1, 2, \dots, T$) is temporarily trained in the corresponding task phase t to recognize target classes \mathcal{C}_t . Following our decoupling strategy, we can reassign the labels of image x_i as:

$$\begin{aligned} \tilde{y}_i^p &= \begin{cases} c_i, & \text{if } y_i^t \in \mathcal{C}_t \vee ((y_i^t = c_b) \wedge (f_{t-1}(x_i) \in \mathcal{C}_{1:t-1})) \\ c'_u, & \text{if } (y_i^t = c_b) \wedge (f_{t-1}(x_i) \notin \mathcal{C}_{1:t-1}) \wedge (S(x_i) = 1), \\ c'_b, & \text{else,} \end{cases} \\ \tilde{y}_i^t &= \begin{cases} y_i^t, & \text{if } y_i^t \in \mathcal{C}_t \\ c_f, & \text{if } (y_i^t = c_b) \wedge (S(x_i) = 1). \\ c'_b, & \text{else,} \end{cases} \end{aligned} \quad (5)$$

Where $f_{t-1}(\cdot)$ is the model of task $t-1$ and $S(\cdot)$ is the salient object detector as used in SSUL (Cha et al., 2021). \tilde{y}_i^p is the label used to train ϕ_p , and \tilde{y}_i^t is the label used to train ϕ_t for the current task t . c_i is the ignored region not included in the loss calculation. The visualization of semantics decoupling is provided in the appendix.

The objective functions for these two branches is defined as:

$$\begin{aligned} \mathcal{L}_p &= \mathcal{L}_{\text{BCE}}(\phi_p(h_\theta(x_i^t)), \tilde{y}_i^p), \\ \mathcal{L}_{\text{current}} &= \mathcal{L}_{\text{BCE}}(\phi_t(h_\theta(x_i^t)), \tilde{y}_i^t). \end{aligned} \quad (6)$$

Finally, the total optimization objective function is:

$$\mathcal{L}_{\text{total}} = \mathcal{L}_{\text{IP}} + \lambda_1 \mathcal{L}_{\text{current}} + \lambda_2 \mathcal{L}_p, \quad (7)$$

where λ_1 and λ_2 are trade-off hyperparameters to balance different training objective functions.

During inference, as illustrated by the green lines in Figure 2, the permanent branch ϕ_p predicts on the background c'_b and unknown objects c'_u , with only c'_b used for inference. Meanwhile, the temporary branch ϕ_t ($t = 1, 2, \dots, T$) predicts for the target classes \mathcal{C}_t , the foreground region c_f and the background c'_b , where \mathcal{C}_t and c_f are used for inference. The pixel-level prediction $\phi_{0:T}(h_\theta(x_i))$ is formulated as:

$$\phi_{0:T}(h_\theta(x_i)) = \text{Concat}(\phi_p(h_\theta(x_i)), \phi_{1:T}(h_\theta(x_i))). \quad (8)$$

Where $\phi_p(h_\theta(x_i))$ and $\phi_{1:T}(h_\theta(x_i))$ represent background prediction from permanent branch and the aggregated foreground predictions from all temporary branches. The pixel-level prediction is then produced by image posterior probability to form the final prediction maps as Eq 3 and Eq 4.

Furthermore, to mitigate the issue of inaccurate predictions on other foreground classes c_f within each task head ϕ_t during inference, we introduce a Noise Filtering trick, filtering out prediction errors associated with c_f . The prediction for the j -th pixel $\hat{y}_{i,j}$ is processed as:

$$\hat{y}_{i,j} = \begin{cases} \alpha_{\text{NF}} \cdot \hat{y}_{i,j} & \text{if } \max(p_{i,j}^f, p_{i,j}^c) = p_{i,j}^f \\ \hat{y}_{i,j} & \text{if } \max(p_{i,j}^f, p_{i,j}^c) = p_{i,j}^c \end{cases} \quad (9)$$

Where α_{NF} is noise filtering term with the default value $\alpha_{\text{NF}} = 0.4$. And $p_{i,j}^f$ and $p_{i,j}^c$ are the j -th pixel logit outputs on the foreground c_f and target class \mathcal{C}_t respectively.

3.5. Improving Memory Buffer

The memory buffer \mathcal{M} plays a crucial role in our implementation and we implement the memory buffer based on unbiased learning and storage efficiency. IPSeg employs a class-balanced sampling strategy, ensuring the image posterior branch can adequately access samples from all classes. Specifically, given the memory size $|\mathcal{M}|$ and the number of already seen classes $|\mathcal{C}_{1:t}|$, the sampling strategy ensures there are at least $|\mathcal{M}| / |\mathcal{C}_{1:t}|$ samples for each class. IPSeg also optimizes the storage cost of \mathcal{M} by only storing image-level labels and object salient masks for samples. Image-level labels are required for the image posterior branch for unbiased classification. While the salient masks split images into background and foreground objects, labeled with 0 and 1 respectively. This simplification mechanism requires less storage cost compared to previous methods that store the whole pixel-wise annotations on all classes. More details can be found in the appendix.

4. Experiments

4.1. Experimental Setups

Dataset Following previous works (Zhang et al., 2023; Cha et al., 2021), we evaluate our method using the Pascal VOC 2012 (Everingham et al., 2010) and ADE20K (Zhou et al., 2017) datasets. Pascal VOC 2012 includes 20 foreground classes and one background class, with 10,582 training images and 1,449 validation images. ADE20K, a larger-scale dataset, comprises 150 classes of stuff and objects, with 20,210 training images and 2,000 validation images.

Protocols We primarily use the *overlap* setting to evaluate our method. This setting is more challenging and realistic than the *disjoint* setting (Qiu et al., 2023), as the images may contain both seen and unseen classes across different

Table 1: Comparison with state-of-the-art methods on Pascal VOC 2012 dataset across 4 typical incremental scenarios. “-” denotes the results are not provided in the original paper. † denotes the result is reproduced using the official code with Swin-B backbone. “IPSeg w/o M” denotes the data-free version of IPSeg, which is trained without memory buffer.

Method		Backbone	VOC 15-5 (2 steps)			VOC 15-1 (6 steps)			VOC 10-1 (11 steps)			VOC 2-2 (10 steps)		
			0-15	16-20	all	0-15	16-20	all	0-10	11-20	all	0-2	3-20	all
Data-free	MiB (Cermelli et al., 2020)	Resnet-101	71.8	43.3	64.7	46.2	12.9	37.9	12.3	13.1	12.7	41.1	23.4	25.9
	SSUL (Cha et al., 2021)	Resnet-101	77.8	50.1	71.2	77.3	36.6	67.6	71.3	46.0	59.3	62.4	42.5	45.3
	IDEC (Zhao et al., 2023)	Resnet-101	78.0	51.8	71.8	77.0	36.5	67.3	70.7	46.3	59.1	-	-	-
	PLOP+NeST (Xie et al., 2024)	Resnet-101	77.6	55.8	72.4	72.2	33.7	63.1	54.2	17.8	36.9	-	-	-
	LAG (Yuan et al., 2024)	Resnet-101	77.3	51.8	71.2	75.0	37.5	66.1	69.6	42.6	56.7	-	-	-
	IPSeg w/o M (ours)	Resnet-101	78.5	55.2	72.9	77.4	41.9	68.9	74.9	52.9	64.4	64.7	51.5	53.4
	SSUL (Cha et al., 2021)	Swin-B	79.7	55.3	73.9	78.1	33.4	67.5	74.3	51.0	63.2	60.3	40.6	44.0
	MicroSeg (Zhang et al., 2022b)	Swin-B	81.9	54.0	75.2	80.5	40.8	71.0	73.5	53.0	63.8	64.8	43.4	46.5
	PLOP+NeST (Xie et al., 2024)	Swin-B	80.5	70.8	78.2	76.8	57.2	72.2	64.3	28.3	47.3	-	-	-
	IPSeg w/o M (ours)	Swin-B	81.4	62.4	76.9	82.4	52.9	75.4	80.0	61.2	71.0	72.1	64.5	65.5
Replay	Joint	Resnet-101	80.5	73.0	78.2	80.5	73.0	78.2	79.1	77.1	78.2	73.9	78.9	78.2
	SDR (Michieli & Zanuttigh, 2021)	Resnet-101	75.4	52.6	69.9	44.7	21.8	39.2	32.4	17.1	25.1	13.0	5.1	6.2
	PLOP-M (Douillard et al., 2021)	Resnet-101	78.5	65.6	75.4	71.1	52.6	66.7	57.9	51.6	54.9	-	-	-
	SSUL-M (Cha et al., 2021)	Resnet-101	79.5	52.9	73.2	78.9	43.9	70.6	74.8	48.9	65.5	58.8	45.8	47.6
	MicroSeg-M (Zhang et al., 2022b)	Resnet-101	82.0	59.2	76.6	81.3	52.5	74.4	77.2	57.2	67.7	60.0	50.9	52.2
	PFCSS-M (Lin et al., 2023)	Resnet-101	79.9	70.2	77.1	77.1	60.4	73.1	69.5	63.2	66.5	-	-	-
	Adapter (Zhu et al., 2024)	Resnet-101	-	-	-	79.9	51.9	73.2	74.9	54.3	65.1	62.8	57.9	58.6
	IPSeg (ours)	Resnet-101	79.5	71.0	77.5	79.6	58.9	74.7	75.9	66.4	71.4	62.4	61.0	61.2
	Joint	Swin-B	83.8	79.3	82.7	83.8	79.3	82.7	82.4	83.0	82.7	75.8	83.9	82.7
SSUL-M† (Cha et al., 2021)	Swin-B	79.3	55.1	73.5	78.8	49.7	71.9	75.3	54.1	65.2	61.1	47.5	49.4	
MicroSeg-M† (Zhang et al., 2022b)	Swin-B	82.9	60.1	77.5	82.0	47.3	73.3	78.9	59.2	70.1	62.7	51.4	53.0	
CoinSeg-M (Zhang et al., 2023)	Swin-B	84.1	69.9	80.8	84.1	65.5	79.6	81.3	64.4	73.7	68.4	65.6	66.0	
IPSeg (ours)	Swin-B	83.3	73.3	80.9	83.5	75.1	81.5	80.3	76.7	78.6	73.1	72.3	72.4	

incremental steps. We evaluate IPSeg under several incremental scenarios, denoted as M - N , where M is the number of classes learned initially, and N is the number of classes learned in each incremental step. For example, VOC 15-1 (6 steps) means learning 15 classes initially and one new class in each subsequent step until all 20 classes are learned. We use the mean Intersection over Union (mIoU) as the evaluation metric.

Implementation details Following previous works (Lin et al., 2022; Baek et al., 2022; Xiao et al., 2023), IPSeg utilizes DeepLab V3 (Chen et al., 2017) as the segmentation model with ResNet-101 (He et al., 2016) and Swin Transformer-base (Swin-B) (Liu et al., 2021) pre-trained on ImageNet-1K (Deng et al., 2009) as the backbones. The training batch size is 16 for Pascal VOC 2012 and 8 for ADE20K. IPSeg uses the SGD optimizer with a momentum of 0.9 and a weight decay of $1e-4$. The learning rates for both datasets are set to 0.01, with learning rate policies of poly for Pascal VOC 2012 and warm poly for ADE20K. All experiments are conducted with 2 NVIDIA GeForce RTX 3090 GPUs. For a fair comparison, the memory size is set as the same as SSUL (Cha et al., 2021) that $|\mathcal{M}| = 100$ for Pascal VOC 2012 and $|\mathcal{M}| = 300$ for ADE20K. Following SSUL (Cha et al., 2021), IPSeg is trained for 50 epochs on Pascal VOC 2012 and 60 epochs on ADE20K. Pseudo-label (Zhang et al., 2023) and saliency information (Hou et al., 2017) are adopted as previous methods (Cha et al.,

2021; Zhang et al., 2022b). To avoid information leaking, the ground truth of the training data in the image posterior branch only consists of annotations and pseudo-labels from the corresponding steps.

Baselines We compare IPSeg with various CISS methods, including MiB (Cermelli et al., 2020), SDR (Michieli & Zanuttigh, 2021), and PLOP (Douillard et al., 2021), as well as state-of-the-art methods such as SSUL (Cha et al., 2021), MicroSeg (Zhang et al., 2022b), PFCSS (Lin et al., 2023), CoinSeg (Zhang et al., 2023), NeST (Xie et al., 2024), LAG (Yuan et al., 2024), and Adapter (Zhu et al., 2024). Among these, PFCSS, CoinSeg, and Adapter are the current state-of-the-art replay methods. For a fair comparison, we reproduce some works using their official code with the Swin-B backbone. Additionally, we provide the results of **Joint** as a theoretical upper bound for incremental tasks. We report incremental results in three parts: initial classes, new classes, and overall classes.

4.2. Main Results

IPSeg is initially designed with a memory buffer \mathcal{M} , enabling it to fully leverage category distribution knowledge from previous samples to mitigate the separate optimization. Consequently, our primary objective is to demonstrate the superiority of IPSeg by comparing it with other replay-based methods, such as “CoinSeg-M”. Additionally, we also

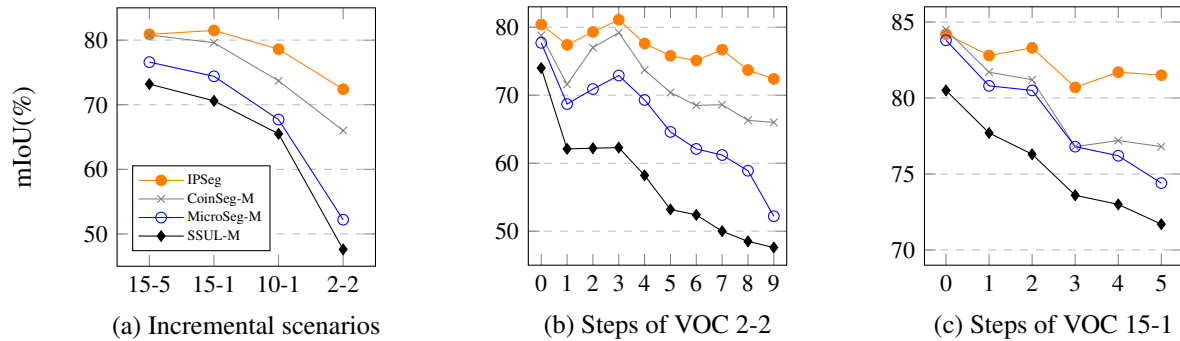


Figure 3: (a) The overall performance of different methods on Pascal VOC 2012 under 4 scenarios, (b) mIoU visualization on Pascal VOC 2012 2-2, (c) mIoU visualization on Pascal VOC 2012 15-1.

present the results of IPSeg without \mathcal{M} (denotes as “IPSeg w/o \mathcal{M} ”) to show the potential and robustness of IPSeg.

Results on Pascal VOC 2012 We evaluate IPSeg in various incremental scenarios on Pascal VOC 2012, including standard incremental scenarios (15-5 and 15-1) and long-term incremental scenarios (10-1 and 2-2). As shown in Table 1, among the replay-based methods, IPSeg achieves the best results across all incremental scenarios on Pascal VOC 2012 with both ResNet-101 and Swin-B backbones. Notably, in the long-term incremental scenarios 10-1 and 2-2, IPSeg achieves performance gains of **4.9%** and **6.4%** over the second-best method, CoinSeg-M, with the same Swin-B backbone. Meanwhile, the data-free version of IPSeg (denotes as “IPSeg w/o \mathcal{M} ”) also demonstrates competitive performance, though without specialized designs.

The superior and robust performance of IPSeg is mainly attributed to the reliable role of guidance provided by the image posterior branch. The image posterior design effectively helps IPSeg avoid catastrophic forgetting and achieve excellent performance on new classes, which often suffer from semantic drift due to separate optimization in new steps. Additionally, the semantics decoupling design enables IPSeg to better learn foreground classes within each incremental step. These designs bring the improvement of **12.3%** and **6.7%** over CoinSeg-M on new classes (11-20) in the 10-1 and 2-2 scenarios, respectively.

Furthermore, as illustrated in Figure 3(a), IPSeg experiences less performance degradation compared to previous state-of-the-art methods as the number of incremental steps increases, which indicates that IPSeg has stronger resistance to catastrophic forgetting. This conclusion is further supported by the data in Figure 3(b) and Figure 3(c), which show that IPSeg exhibits minimal performance declines as the incremental process continues. In contrast, other methods only maintain comparable performance during the initial incremental learning step but quickly degrade in subsequent steps due to catastrophic forgetting. This detailed trend of

performance decline across steps validates the effectiveness and robustness of IPSeg in resisting forgetting.

Results on ADE20K We also conduct a comparison between IPSeg and its competitors under different incremental scenarios on the more challenging ADE20K dataset with two backbones. As shown in Table 2, IPSeg consistently achieves performance advantages compared with other replay-based methods, which is similar to those observed on Pascal VOC 2012. Notably, IPSeg with Swin-B backbone demonstrates more significant improvements over its competitors across all incremental scenarios on the ADE20K dataset, with the smallest improvement of **2.1%** in the 100-5 scenario and the largest improvement of **6.0%** in the 100-50 scenario. The superior performance on the more realistic and complex ADE20K dataset further demonstrates the effectiveness and robustness of IPSeg.

4.3. Ablation Study

Ablation on IP branch The image posterior (IP) branch is trained incrementally but faces challenges due to the lack of labels for old classes. To address this issue, we employ image-level pseudo-label $\tilde{y}_i^{m,t}$ (PL) instead of directly using the partial ground truth label $y_i^{m,t}$, providing comprehensive supervision at the risk of introducing noise due to the inconsistencies between previous heads predictions and current training labels. As shown in Table 3, our method achieves significant improvement compared to using only partial ground truth (Part-GT), and narrows the gap with the upper bound (Full-GT). This indicates that using $\tilde{y}_i^{m,t}$ is an efficient trade-off, where the benefits of additional supervision from pseudo labels outweigh the potential noise. With this training design, the image posterior branch helps IPSeg effectively mitigate separate optimization and shows superior performance.

Ablation on proposed components We analyze the effect of the components in IPSeg, including Image Posterior (IP), Semantics Decoupling (SD), and the Noise Filtering (NF)

Table 2: Comparison with state-of-the-art methods on ADE20K dataset. † denotes the result is reproduced using the official code with Swin-B backbone. * denotes the results from a longer training schedule of 100 epochs, while 60 epochs in ours.

Method		Backbone	ADE 100-5 (11 steps)			ADE 100-10 (6 steps)			ADE 100-50 (2 steps)			ADE 50-50 (3 steps)		
			0-100	101-150	all	0-100	101-150	all	0-100	101-150	all	0-50	51-150	all
Data-free	MiB (Cermelli et al., 2020)	Resnet-101	36.0	5.7	26.0	38.2	11.1	29.2	40.5	17.2	32.8	45.6	21.0	29.3
	SSUL (Cha et al., 2021)	Resnet-101	39.9	17.4	32.5	40.2	18.8	33.1	41.3	18.0	33.6	48.4	20.2	29.6
	MicroSeg (Zhang et al., 2022b)	Resnet-101	40.4	20.5	33.8	41.5	21.6	34.9	40.2	18.8	33.1	48.6	24.8	32.9
	IDEC (Zhao et al., 2023)	Resnet-101	39.2	14.6	31.0	40.3	17.6	32.7	42.0	18.2	34.1	47.4	26.0	33.1
	AWT+MiB (Goswami et al., 2023)	Resnet-101	38.6	16.0	31.1	39.1	21.4	33.2	40.9	24.7	35.6	46.6	27.0	33.5
	PLOP+NeST (Xie et al., 2024)	Resnet-101	39.3	17.4	32.0	40.9	22.0	34.7	42.2	24.3	36.3	48.7	27.7	34.8
	BAM (Zhang & Gao, 2025)	Resnet-101	40.5	21.1	34.1	41.1	23.1	35.2	42.0	23.0	35.7	47.9	26.5	33.7
	IPSeg w/o M (ours)	Resnet-101	41.0	22.4	34.8	41.0	23.6	35.3	41.3	24.0	35.5	46.7	26.2	33.1
	SSUL† (Cha et al., 2021)	Swin-B	41.3	16.0	32.9	40.7	19.0	33.5	41.9	20.1	34.6	49.5	21.3	30.7
	CoinSeg (Zhang et al., 2023)	Swin-B	43.1	24.1	36.8	42.1	24.5	36.2	41.6	26.7	36.6	49.0	28.9	35.6
PLOP+NeST (Xie et al., 2024)	Swin-B	39.7	18.3	32.6	41.7	24.2	35.9	43.5	26.5	37.9	50.6	28.9	36.2	
IPSeg w/o M (ours)	Swin-B	43.1	26.2	37.6	42.5	27.8	37.6	43.2	29.0	38.4	49.3	33.0	38.5	
Replay	Joint	Resnet-101	43.5	29.4	38.3	43.5	29.4	38.8	43.5	29.4	38.8	50.3	32.7	38.8
	SSUL-M (Cha et al., 2021)	Resnet-101	42.9	17.8	34.6	42.9	17.7	34.5	42.8	17.5	34.4	49.1	20.1	29.8
	TIKP (Yu et al., 2024)	Resnet-101	37.5	17.6	30.9	41.0	19.6	33.8	42.2	20.2	34.9	48.8	25.9	33.6
	Adapter* (Zhu et al., 2024)	Resnet-101	42.6	18.0	34.5	42.9	19.9	35.3	43.1	23.6	36.7	49.3	27.3	34.7
	IPSeg (ours)	Resnet-101	42.4	22.7	35.9	42.1	22.3	35.6	41.7	25.2	36.3	47.3	26.7	33.6
	Joint	Swin-B	47.2	31.9	42.1	47.2	31.9	42.1	47.2	31.9	42.1	54.6	35.5	42.1
	SSUL-M† (Cha et al., 2021)	Swin-B	41.6	20.1	34.5	41.6	19.9	34.4	41.5	48.0	33.7	47.6	18.8	28.5
	CoinSeg-M† (Zhang et al., 2023)	Swin-B	42.8	24.8	36.8	39.6	24.8	34.7	38.7	23.7	33.7	48.8	28.9	35.4
IPSeg (ours)	Swin-B	43.2	30.4	38.9	43.0	30.9	39.0	43.8	31.5	39.7	51.1	34.8	40.3	

Table 3: Ablation on different label choices to incrementally train the image posterior branch.

Methods	Labels		VOC 15-5 (2 steps)			VOC 10-1 (11 steps)			VOC 2-2 (10 steps)		
	$\mathcal{C}_{1:t-1}$	\mathcal{C}_t	0-15	16-20	all	0-10	11-20	all	0-2	3-20	all
Part-GT	X	GT	83.3	72.8	80.8	79.3	74.5	77.0	72.6	69.4	69.8
Pseudo (ours)	PL	GT	83.3	73.3	80.9	80.3	76.7	78.6	73.1	72.3	72.4
Full-GT	GT	GT	83.2	73.8	81.0	80.1	78.0	79.2	75.2	74.6	74.8

Table 4: Overall ablation study for IPSeg on VOC 15-1.

IP	SD	NF	VOC 15-1 (6 steps)		
			0-15	16-20	all
X	X	X	78.8	49.7	71.9
✓	X	X	79.4	69.6	77.0 \uparrow 5.1
X	✓	X	83.1	65.1	78.8 \uparrow 6.9
✓	✓	X	83.4	74.7	81.3 \uparrow 9.4
✓	✓	✓	83.6	75.1	81.6 \uparrow 9.7

in SD. All ablations are implemented in Pascal VOC 2012 using the Swin-B backbone. As shown in Table 4, the second row indicates that **IP** brings significant improvement to new classes. Benefiting from **IP**'s ability to align probability scales between different task heads, the reliable guidance prevents model performance from degradation caused by *separate optimization*. The third row shows the excellent ability of **SD** in learning foreground targets at each step by effective decoupling. The fourth and fifth rows demonstrate IPSeg's outstanding performance on both old and new

classes using **IP** and **SD** together. More ablation studies and visualization results for IPSeg are provided in the appendix.

5. Conclusions and Limitations

In this paper, We propose IPSeg, a simple yet effective method designed to address the issue of semantic drift in class incremental semantic segmentation. We begin by analyzing the details of semantic drift, identifying two key issues: separate optimization and noisy semantics. To mitigate these issues, IPSeg introduces two specific designs: image posterior guidance and semantics decoupling. Experimental results on the Pascal VOC 2012 and ADE20K datasets demonstrate the superior performance of our method, particularly in long-term incremental scenarios.

Limitations While IPSeg introduces a novel and promising approach for the class incremental semantic segmentation challenge, We have to claim that IPSeg is based upon the memory buffer for improving classification ability. The basis limits its potential in privacy-sensitive scenarios. Eliminating the need for a memory buffer and extending IPSeg to a wider range of applications are our future targets.

Impact Statement

Though IPSeg exhibits superior performance and properties of learning plasticity and memory stability, we realize that the usage of memory buffer leaves a lot of room for discussion. On the one hand, the use of memory buffers brings additional storage costs and the risk of information leakage. On the other hand, the use of memory buffers is related to privacy issues in some cases, such as storing private information without approval. These issues need to be treated with caution in artificial intelligence applications.

References

- Baek, D., Oh, Y., Lee, S., Lee, J., and Ham, B. Decomposed knowledge distillation for class-incremental semantic segmentation. *Advances in Neural Information Processing Systems*, 35:10380–10392, 2022.
- Bang, J., Kim, H., Yoo, Y., Ha, J.-W., and Choi, J. Rainbow memory: Continual learning with a memory of diverse samples. In *Proceedings of the IEEE/CVF conference on computer vision and pattern recognition*, pp. 8218–8227, 2021.
- Belouadah, E. and Popescu, A. Il2m: Class incremental learning with dual memory. In *Proceedings of the IEEE/CVF international conference on computer vision*, pp. 583–592, 2019.
- Buzzega, P., Boschini, M., Porrello, A., Abati, D., and Calderara, S. Dark experience for general continual learning: a strong, simple baseline. *Advances in neural information processing systems*, 33:15920–15930, 2020.
- Camuffo, E. and Milani, S. Continual learning for lidar semantic segmentation: Class-incremental and coarse-to-fine strategies on sparse data. In *Proceedings of the IEEE/CVF Conference on Computer Vision and Pattern Recognition*, pp. 2447–2456, 2023.
- Cermelli, F., Mancini, M., Bulò, S. R., Ricci, E., and Caputo, B. Modeling the background for incremental learning in semantic segmentation. In *Proceedings of the IEEE/CVF Conference on Computer Vision and Pattern Recognition*, pp. 9233–9242, 2020.
- Cha, S., Yoo, Y., Moon, T., et al. Ssul: Semantic segmentation with unknown label for exemplar-based class-incremental learning. *Advances in neural information processing systems*, 34:10919–10930, 2021.
- Chen, J., Wang, Y., Wang, P., Chen, X., Zhang, Z., Lei, Z., and Li, Q. Diffusepast: Diffusion-based generative replay for class incremental semantic segmentation. *arXiv preprint arXiv:2308.01127*, 2023.
- Chen, L.-C., Papandreou, G., Schroff, F., and Adam, H. Rethinking atrous convolution for semantic image segmentation. *arXiv preprint arXiv:1706.05587*, 2017.
- De Lange, M., Aljundi, R., Masana, M., Parisot, S., Jia, X., Leonardis, A., Slabaugh, G., and Tuytelaars, T. A continual learning survey: Defying forgetting in classification tasks. *IEEE transactions on pattern analysis and machine intelligence*, 44(7):3366–3385, 2021.
- Deng, J., Dong, W., Socher, R., Li, L.-J., Li, K., and Fei-Fei, L. Imagenet: A large-scale hierarchical image database. In *2009 IEEE conference on computer vision and pattern recognition*, pp. 248–255. Ieee, 2009.
- Douillard, A., Cord, M., Ollion, C., Robert, T., and Valle, E. Podnet: Pooled outputs distillation for small-tasks incremental learning. In *Computer vision—ECCV 2020: 16th European conference, Glasgow, UK, August 23–28, 2020, proceedings, part XX 16*, pp. 86–102. Springer, 2020.
- Douillard, A., Chen, Y., Dapogny, A., and Cord, M. Plop: Learning without forgetting for continual semantic segmentation. In *Proceedings of the IEEE/CVF conference on computer vision and pattern recognition*, pp. 4040–4050, 2021.
- Douillard, A., Ramé, A., Couairon, G., and Cord, M. Dytox: Transformers for continual learning with dynamic token expansion. In *Proceedings of the IEEE/CVF Conference on Computer Vision and Pattern Recognition*, pp. 9285–9295, 2022.
- Everingham, M., Van Gool, L., Williams, C. K., Winn, J., and Zisserman, A. The pascal visual object classes (voc) challenge. *International journal of computer vision*, 88: 303–338, 2010.
- Goodfellow, I., Pouget-Abadie, J., Mirza, M., Xu, B., Warde-Farley, D., Ozair, S., Courville, A., and Bengio, Y. Generative adversarial networks. *Communications of the ACM*, 63(11):139–144, 2020.
- Goswami, D., Schuster, R., van de Weijer, J., and Stricker, D. Attribution-aware weight transfer: A warm-start initialization for class-incremental semantic segmentation. In *Proceedings of the IEEE/CVF Winter Conference on Applications of Computer Vision*, pp. 3195–3204, 2023.
- Gurbuz, M. B. and Dvornik, C. Nispa: Neuro-inspired stability-plasticity adaptation for continual learning in sparse networks. *arXiv preprint arXiv:2206.09117*, 2022.
- He, K., Zhang, X., Ren, S., and Sun, J. Deep residual learning for image recognition. In *Proceedings of the IEEE conference on computer vision and pattern recognition*, pp. 770–778, 2016.

- Ho, J., Jain, A., and Abbeel, P. Denoising diffusion probabilistic models. *Advances in neural information processing systems*, 33:6840–6851, 2020.
- Hou, Q., Cheng, M.-M., Hu, X., Borji, A., Tu, Z., and Torr, P. H. Deeply supervised salient object detection with short connections. In *Proceedings of the IEEE conference on computer vision and pattern recognition*, pp. 3203–3212, 2017.
- Jung, S., Ahn, H., Cha, S., and Moon, T. Continual learning with node-importance based adaptive group sparse regularization. *Advances in neural information processing systems*, 33:3647–3658, 2020.
- Ke, Z. and Liu, B. Continual learning of natural language processing tasks: A survey. *arXiv preprint arXiv:2211.12701*, 2022.
- Kim, B., Yu, J., and Hwang, S. J. Eclipse: Efficient continual learning in panoptic segmentation with visual prompt tuning. In *Proceedings of the IEEE/CVF Conference on Computer Vision and Pattern Recognition*, pp. 3346–3356, 2024.
- Kirkpatrick, J., Pascanu, R., Rabinowitz, N., Veness, J., Desjardins, G., Rusu, A. A., Milan, K., Quan, J., Ramalho, T., Grabska-Barwinska, A., et al. Overcoming catastrophic forgetting in neural networks. *Proceedings of the national academy of sciences*, 114(13):3521–3526, 2017.
- Kudithipudi, D., Aguilar-Simon, M., Babb, J., Bazhenov, M., Blackiston, D., Bongard, J., Brna, A. P., Chakravarthi Raja, S., Cheney, N., Clune, J., et al. Biological underpinnings for lifelong learning machines. *Nature Machine Intelligence*, 4(3):196–210, 2022.
- Li, Z. and Hoiem, D. Learning without forgetting. *IEEE transactions on pattern analysis and machine intelligence*, 40(12):2935–2947, 2017.
- Lin, Z., Wang, Z., and Zhang, Y. Continual semantic segmentation via structure preserving and projected feature alignment. In *European Conference on Computer Vision*, pp. 345–361. Springer, 2022.
- Lin, Z., Wang, Z., and Zhang, Y. Preparing the future for continual semantic segmentation. In *Proceedings of the IEEE/CVF International Conference on Computer Vision*, pp. 11910–11920, 2023.
- Liu, X., Wu, C., Menta, M., Herranz, L., Raducanu, B., Bagdanov, A. D., Jui, S., and de Weijer, J. v. Generative feature replay for class-incremental learning. In *Proceedings of the IEEE/CVF Conference on Computer Vision and Pattern Recognition Workshops*, pp. 226–227, 2020.
- Liu, Z., Lin, Y., Cao, Y., Hu, H., Wei, Y., Zhang, Z., Lin, S., and Guo, B. Swin transformer: Hierarchical vision transformer using shifted windows. In *Proceedings of the IEEE/CVF international conference on computer vision*, pp. 10012–10022, 2021.
- Mai, Z., Li, R., Jeong, J., Quispe, D., Kim, H., and Sanner, S. Online continual learning in image classification: An empirical survey. *Neurocomputing*, 469:28–51, 2022.
- Maracani, A., Michieli, U., Toldo, M., and Zanuttigh, P. Recall: Replay-based continual learning in semantic segmentation. In *Proceedings of the IEEE/CVF international conference on computer vision*, pp. 7026–7035, 2021.
- McClelland, J. L., McNaughton, B. L., and O’Reilly, R. C. Why there are complementary learning systems in the hippocampus and neocortex: insights from the successes and failures of connectionist models of learning and memory. 102(3):419, 1995.
- McCloskey, M. and Cohen, N. J. Catastrophic interference in connectionist networks: The sequential learning problem. In *Psychology of learning and motivation*, volume 24, pp. 109–165. Elsevier, 1989.
- Michieli, U. and Zanuttigh, P. Continual semantic segmentation via repulsion-attraction of sparse and disentangled latent representations. In *Proceedings of the IEEE/CVF conference on computer vision and pattern recognition*, pp. 1114–1124, 2021.
- Phan, M. H., Phung, S. L., Tran-Thanh, L., Bouzerdoum, A., et al. Class similarity weighted knowledge distillation for continual semantic segmentation. In *Proceedings of the IEEE/CVF Conference on Computer Vision and Pattern Recognition*, pp. 16866–16875, 2022.
- Qiu, Y., Shen, Y., Sun, Z., Zheng, Y., Chang, X., Zheng, W., and Wang, R. Sats: Self-attention transfer for continual semantic segmentation. *Pattern Recognition*, 138:109383, 2023.
- Qu, H., Rahmani, H., Xu, L., Williams, B., and Liu, J. Recent advances of continual learning in computer vision: An overview. *arXiv preprint arXiv:2109.11369*, 2021.
- Rebuffi, S.-A., Kolesnikov, A., Sperl, G., and Lampert, C. H. icarl: Incremental classifier and representation learning. In *Proceedings of the IEEE conference on Computer Vision and Pattern Recognition*, pp. 2001–2010, 2017.
- Serra, J., Suris, D., Miron, M., and Karatzoglou, A. Overcoming catastrophic forgetting with hard attention to the task. In *International conference on machine learning*, pp. 4548–4557. PMLR, 2018.

- Shin, H., Lee, J. K., Kim, J., and Kim, J. Continual learning with deep generative replay. *Advances in neural information processing systems*, 30, 2017.
- Silver, D. L., Yang, Q., and Li, L. Lifelong machine learning systems: Beyond learning algorithms. In *2013 AAAI spring symposium series*, 2013.
- Wang, L., Xie, J., Zhang, X., Huang, M., Su, H., and Zhu, J. Hierarchical decomposition of prompt-based continual learning: Rethinking obscured sub-optimality. *Advances in Neural Information Processing Systems*, 36, 2024a.
- Wang, L., Zhang, X., Su, H., and Zhu, J. A comprehensive survey of continual learning: Theory, method and application. *IEEE Transactions on Pattern Analysis and Machine Intelligence*, 2024b.
- Xiao, J.-W., Zhang, C.-B., Feng, J., Liu, X., van de Weijer, J., and Cheng, M.-M. Endpoints weight fusion for class incremental semantic segmentation. In *Proceedings of the IEEE/CVF Conference on Computer Vision and Pattern Recognition*, pp. 7204–7213, 2023.
- Xie, Z., Lu, H., Xiao, J.-w., Wang, E., Zhang, L., and Liu, X. Early preparation pays off: New classifier pre-tuning for class incremental semantic segmentation. *arXiv preprint arXiv:2407.14142*, 2024.
- Yu, Z., Yang, W., Xie, X., and Shi, Z. Tikp: Text-to-image knowledge preservation for continual semantic segmentation. In *Proceedings of the AAAI Conference on Artificial Intelligence*, volume 38, pp. 16596–16604, 2024.
- Yuan, B. and Zhao, D. A survey on continual semantic segmentation: Theory, challenge, method and application. *arXiv preprint arXiv:2310.14277*, 2023.
- Yuan, B., Zhao, D., and Shi, Z. Learning at a glance: Towards interpretable data-limited continual semantic segmentation via semantic-invariance modelling. *IEEE Transactions on Pattern Analysis and Machine Intelligence*, 2024.
- Zhang, A. and Gao, G. Background adaptation with residual modeling for exemplar-free class-incremental semantic segmentation. In *European Conference on Computer Vision*, pp. 166–183. Springer, 2025.
- Zhang, C.-B., Xiao, J.-W., Liu, X., Chen, Y.-C., and Cheng, M.-M. Representation compensation networks for continual semantic segmentation. In *Proceedings of the IEEE/CVF Conference on Computer Vision and Pattern Recognition*, pp. 7053–7064, 2022a.
- Zhang, Z., Gao, G., Fang, Z., Jiao, J., and Wei, Y. Mining unseen classes via regional objectness: A simple baseline for incremental segmentation. *Advances in neural information processing systems*, 35:24340–24353, 2022b.
- Zhang, Z., Gao, G., Jiao, J., Liu, C. H., and Wei, Y. Coinseg: Contrast inter-and intra-class representations for incremental segmentation. In *Proceedings of the IEEE/CVF International Conference on Computer Vision*, pp. 843–853, 2023.
- Zhao, D., Yuan, B., and Shi, Z. Inherit with distillation and evolve with contrast: Exploring class incremental semantic segmentation without exemplar memory. *IEEE Transactions on Pattern Analysis and Machine Intelligence*, 2023.
- Zhou, B., Zhao, H., Puig, X., Fidler, S., Barriuso, A., and Torralba, A. Scene parsing through ade20k dataset. In *Proceedings of the IEEE conference on computer vision and pattern recognition*, pp. 633–641, 2017.
- Zhu, G., Wu, D., Gao, C., Wang, R., Yang, W., and Sang, N. Adaptive prototype replay for class incremental semantic segmentation. *arXiv preprint arXiv:2412.12669*, 2024.

A. Appendix

A.1. Symbols and Explanations

Table 5 provides key symbols used in our paper along with their explanations to facilitate a better understanding.

Table 5: Symbols and explanations

Symbol	Explanations	
Model architecture	f_t	Model of task t .
	h_θ	The backbone extracting features.
	$\phi_{1:t}$	All segmentation heads, outputting the final results.
	ϕ_t	The head of task t , representing the temporary branch.
	ϕ_p	The permanent branch.
	ψ	The image posterior branch.
Semantic concepts	\mathcal{C}_t	The target classes set of task t .
	$\mathcal{C}_{1:t-1}$	The old classes set.
	c'_b	The pure background.
	c'_u	Unknown foreground.
	c_i	The ignored region that does not participate in loss calculation.
	c_f	The foreground regions that do not belong to target classes \mathcal{C}_t .
	c_u	Unknown classes defined in previous methods, consisting of $\mathcal{C}_{1:t-1}$ and c'_u .
c_b	The background defined in previous methods, consisting of c'_b and c_u .	
Data and label	\mathcal{D}_t	Training dataset of current incremental task t .
	\mathcal{M}	Memory buffer, with fixed size of 100 for Pascal VOC and 300 for ADE20K.
	x_i^t	The i -th image in \mathcal{D}_t .
	y_i^t	The pixel annotations of x_i^t .
	$x_i^{m,t}$	The mixed data selected from \mathcal{M} and \mathcal{D}_t .
	$\tilde{y}_i^{m,t}$	The image-level pseudo-label of $x_i^{m,t}$.
	\tilde{y}_i^p	Label assigned to the permanent branch ϕ_p .
	\tilde{y}_i^t	Label assigned to the temporary branch ϕ_t .

A.2. Observation

Visualization of separate optimization As shown in Figure 4, to illustrate the inconsistent outputs caused by *separate optimization*, we select three pairs of similar classes from Pascal VOC 2012: “cow” and “horse”, “bus” and “car”, “sofa” and “chair”, and split them into two separate groups for learning. Sequence B follows a reverse learning order compared to Sequence A, and the goal is to examine the model’s final predictions with different learning sequence. Columns A and B are the models’ final predictions of sequence A and sequence B respectively. These visualizations indicate that the earlier head of the model tends to produce high scores for certain classes, regardless of the learning order, suggesting that *separate optimization* causes a persistent bias towards the classes learned first.

Impact of IPSeg on separate optimization To validate the impact of IPSeg on *separate optimization*, we calculate the average probability distribution of the incorrect prediction area (red box in the image) as depicted in Figure 5. SSUL-M misclassifies the little sheep as cow with abnormal probability distribution. In contrast, IPSeg utilizes image posterior guidance to produce more accurate and harmonious prediction. Compared to previous works, IPseg maintains a harmonious

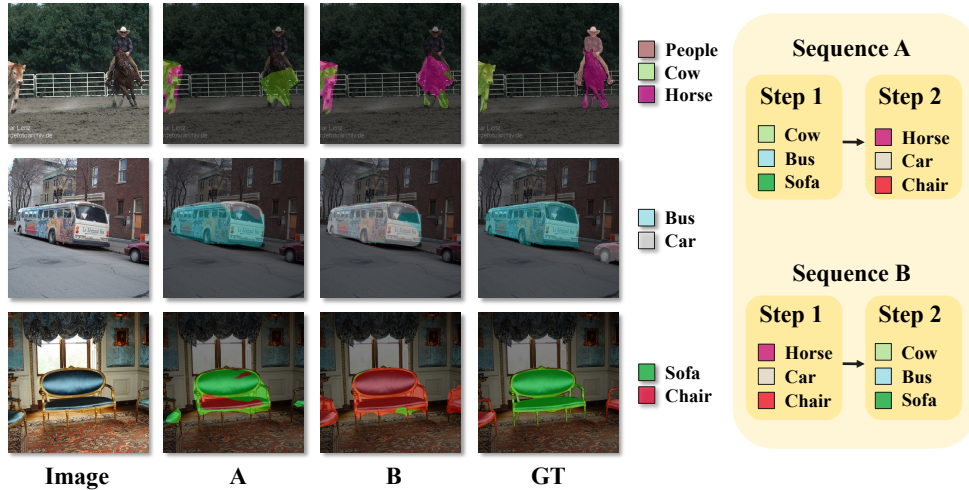


Figure 4: The visualization of separate optimization. *Sequence A*: first learn “cow”, “bus”, “sofa” in step 1, then “horse”, “car”, “chair” in step 2. *Sequence B*: first learn “horse”, “car”, “chair” in step 1, then “cow”, “bus”, “sofa” in step 2.

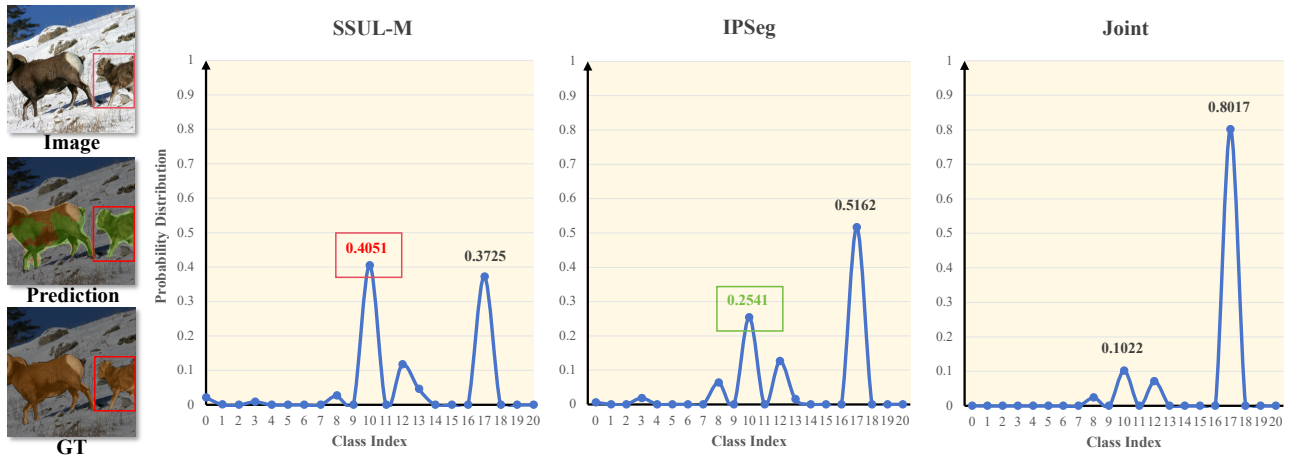


Figure 5: The probability distributions for SSUL-M, IPSeg, and Joint-Training (Joint) in the regions of incorrect predictions. Class indexes “10” and “17” represent “cow” and “sheep” respectively.

and realistic probability distribution more similar to that of the theoretical upper bound, Joint-Training (Joint), demonstrating its superior capability in dealing with *separate optimization*.

Visualization of semantics decoupling Figure 6 is the semantics decoupling illustration for image x_i^t . In this case, the current classes \mathcal{C}_t “person” is provided with ground truth as y_i^t . The foreground classes “sofa” and “cat”, however, are unknown without ground truth. IPSeg uses a saliency map to locate the current unknown object “sofa” and “cat” as other foregrounds c_f and further utilizes pseudo label to distinguish “sofa” as unknown foreground c'_u . It is worth noting that the regions of “person” and “cat” belong to the ignored regions c_i that do not participate in loss calculation. In this way, the remaining region is labeled as “pure” background c'_b . The “pure” background c'_b and unknown foreground c'_u are considered as static and permanent concepts. The target classes \mathcal{C}_t with ground truth y_i^t and other foreground c_f are considered as dynamic and temporary concepts.

Qualitative analysis of IPSeg Figure 7 presents a qualitative analysis of IPSeg compared with SSUL-M and CoinSeg-M. Visualization results are from each incremental step in the VOC 2-2 scenario. The results in rows 1, 3, and 5 demonstrate that both SSUL-M and CoinSeg-M mistakenly predict “horse” as “cow” at step 6, while IPSeg correctly identifies “horse”.

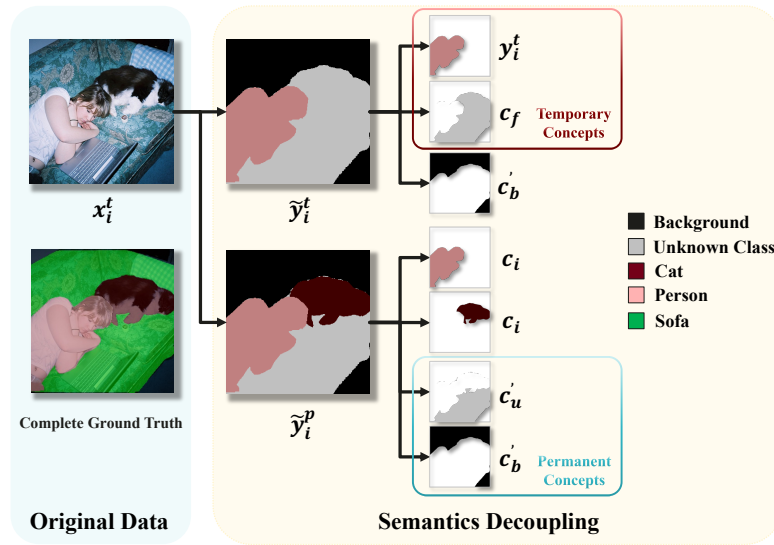


Figure 6: Semantics decoupling strategy

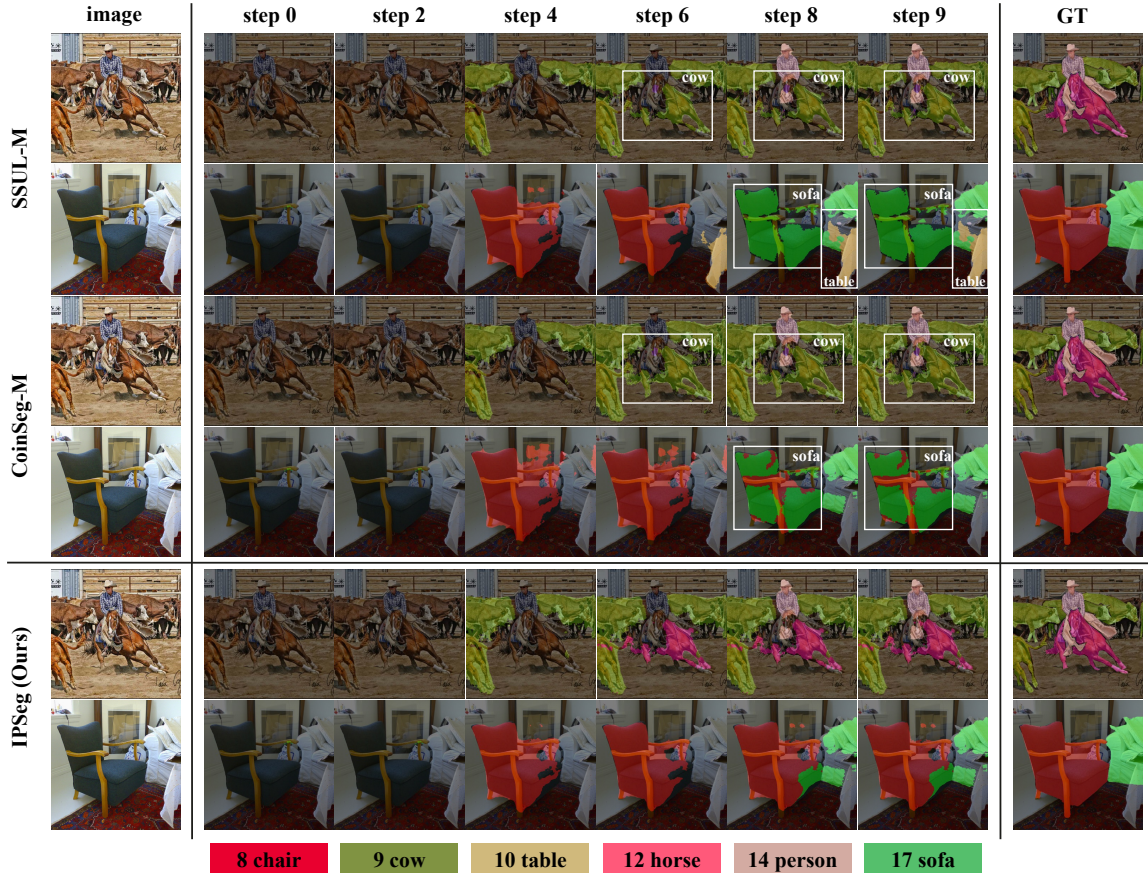


Figure 7: Qualitative analysis of IPSeg on Pascal VOC 2012. Texts and bounding boxes in white indicate incorrect class predictions starting from the corresponding incremental step. Color-shaded boxes with classes and indexes represent the learned classes in the corresponding learning steps.

In rows 2, 4, and 6, IPSeg consistently predicts the old class “chair”, whereas SSUL-M predicts “sofa” as “table” at step 6, and both SSUL-M and CoinSeg-M mistake “chair” for “sofa” at step 8. These visualization results reveal that IPSeg not only achieves excellent learning plasticity but also maintains strong memory stability.

A.3. Additional Results and Analysis

Evaluation on image-level predictions To investigate the ability to resist catastrophic forgetting of the image posterior (IP) branch and the segmentation branch, we evaluate the image level accuracy performance of the base 15 classes using the IP branch and the segmentation branch at each step on Pascal VOC 15-1 as shown in Table 6. “IP” refers to the image-level accuracy of the IP branch, “Pixel” refers to the image-level accuracy of the segmentation branch, where class C exists if a pixel is predicted as C . “Pixel+IP” denotes the final result of IPSeg. The ablation shows that: the image-level performance suffers less forgetting than the segmentation, and our method shows similar property against forgetting with the help of IP.

Table 6: The image-level accuracy of IP branch and the segmentation branch on 15 base classes.

ACC (%)	step 0	step 1	step 2	step 3	step 4	step 5
IP	87.44	86.41	86.99	86.82	86.86	86.29
Pixel	88.17	86.42	86.30	85.43	84.84	84.70
Pixel+IP	93.07	92.24	92.41	91.93	91.95	91.02

We also present the image-level accuracy on all seen classes at each step to analyze their performance on both old classes and new classes in Table 7. For the segmentation branch, the image-level accuracy of it on all seen classes gradually degrades after learning new classes, performing worse than its accuracy on base classes. This indicates the segmentation branch performs poorly on new classes, which is consistent with our description about separate optimization. In contrast, the IP branch experiences less deterioration from separate optimization and help our method maintain a good balance between retaining old knowledge and learning new knowledge.

Table 7: The image-level accuracy of IP branch and the segmentation branch on all seen classes.

ACC (%)	step 0	step 1	step 2	step 3	step 4	step 5 (Final)
IP	87.44	82.54	81.14	81.32	82.09	82.34
Pixel	88.17	83.56	82.29	78.23	77.60	76.57
Pixel+IP	93.07	90.05	90.13	87.30	87.68	88.03

Evaluation on model parameters, training and inference costs We provide a comprehensive analysis of the model parameters, training, and inference costs as shown in Table 8. We test and report the results of IPSeg, SSUL-M and CoinSeg-M with Swin-B on the VOC 15-1 setting. We set $image_size=512 \times 512$, $epochs=50$, and $batch_size=16$ in training and $image_size=512 \times 512$ for inference test. All results are run on RTX 3090 GPU.

- **Model Parameters:** Using the thop tool, we analyze and compare the trainable parameters for these methods. The sizes of increased parameters in them are close, with average 3.84M per step. Additionally, IPSeg has 29.72M parameters more than SSUL due to the additional image posterior branch.
- **Training:** Due to the introduced image posterior branch, IPSeg needs more training cost compared with SSUL-M but less than CoinSeg-M.
- **Inference:** The inference speed of IPSeg (27.3 FPS) is slightly lower than SSUL-M (33.7 FPS) and similar to CoinSeg-M (28.2 FPS). Due to the proposed image posterior branch, the model’s floating-point operations (137.1 GFLOPs) are higher than the baseline (94.9 GFLOPs), and with an approximately 1 GB increase in GPU usage. Note that the increase in FLOPs mainly stems from IPSeg’s use of image-level predictions to guide final outputs. Specifically, IPSeg broadcasts image-level predictions to match the shape of pixel-level logits and combines them through element-wise multiplication, which are inherently parallelizable and can be optimized and accelerated by GPUs, ensuring that the inference speed remains largely unaffected.

Overall, IPSeg introduces an additional image posterior branch with slight increases in model parameters, training cost, and inference but brings great performance improvement. It is a worthwhile trade-off between performance and cost.

Table 8: Comparison of IPSeg with baseline on model parameters, training and inference costs.

Method	Incremental Steps						Training		Inference		
	0	1	2	3	4	5	Time	GPU usage	FPS	FLOPs	GPU usage
IPseg	135.92 M	139.76 M	143.60 M	147.66 M	151.28 M	155.12 M	9h 14min	21.1G	27.3	137.1G	6.2G
SSUL-M	106.20 M	110.03 M	113.89 M	117.95 M	121.56 M	125.40 M	7h 13min	19.4G	33.7	94.9G	5.3G
CoinSeg-M	107.02 M	111.15 M	115.29 M	119.42 M	123.55 M	127.68 M	> 15h	21.3G	28.2	96.3G	5.6G

The details of efficient data storage in memory buffer For raw data, IPSeg directly stores the image paths in a JSON file, as done in previous works (Cha et al., 2021; Zhang et al., 2022b; 2023). For image-level labels, IPSeg stores the class labels of the images as arrays in the same JSON file with multi-hot encoding, where 1 indicates the presence of a class and 0 indicates absence. The memory cost for this is negligible. For pixel-level labels, instead of storing full-class annotations (with a data type of *uint8*) as prior approaches, IPSeg only stores the salient mask, where the background and foreground are labeled as 0 and 1, respectively (with a data type of *bool*). Theoretically, the storage space could be reduced to 1/8.

Ablation study on memory buffer Since IPSeg is designed for data-replay scenarios, the IP branch heavily relies on a memory buffer. To evaluate the impact of the memory buffer on performance, we compare the standard version of IPSeg with a data-free variant (denoted as IPSeg w/o M). As shown in Table 9, IPSeg demonstrates competitive performance even without the memory buffer. However, the performance gap between the data-free and data-replay settings highlights the essential role of the memory buffer in enhancing IPSeg’s effectiveness.

Table 9: Comparison with other methods in data-free version using Swin-B backbone.

Method	VOC 15-5 (2 steps)			VOC 15-1 (6 steps)			VOC 10-1 (11 steps)			VOC 2-2 (10 steps)		
	0-15	16-20	all	0-15	16-20	all	0-10	11-20	all	0-2	3-20	all
SSUL	79.7	55.3	73.9	78.1	33.4	67.5	74.3	51.0	63.2	60.3	40.6	44.0
MicroSeg	81.9	54.0	75.2	80.5	40.8	71.0	73.5	53.0	63.8	64.8	43.4	46.5
IPSeg w/o M	81.4	62.4	76.9	82.4	52.9	75.4	80.0	61.2	71.0	72.1	64.5	65.5
IPSeg w/ M	83.3	73.3	80.9	83.5	75.1	81.5	80.3	76.7	78.6	73.1	72.3	72.4

Ablation study for hyper-parameters: weight terms of loss. We conduct an ablation study on the two weight terms λ_1 and λ_2 , testing values of 0.1, 0.25, 0.5, 0.75, and 1.0. The results are shown in Table 10. It is obvious that the setting of $\lambda_1 = 0.5$ and $\lambda_2 = 0.5$ achieves the best performance, which is the default value of IPSeg.

Ablation study of hyper-parameters Table 11(a) and (b) illustrate the effects of hyper-parameters: memory size $|\mathcal{M}|$, the strength of noise filtering α_{NF} , and background compensation α_{BC} , which shows that IPseg is not sensitive to the value of α_{NF} and α_{BC} and we set the default values for these parameters to $|\mathcal{M}| = 100$, $\alpha_{NF} = 0.4$ and $\alpha_{BR} = 0.9$.

Table 10: Ablation Studies on Pascal VOC 15-1 task for hyper-parameters: weight terms of loss, λ_1 and λ_2 .

$\lambda_1 \setminus \lambda_2$	0.1	0.25	0.5	0.75	1.0
0.1	79.2	80.3	80.4	80.8	78.0
0.25	79.8	80.3	81.1	81.0	80.9
0.5	80.3	80.9	81.5	81.2	80.9
0.75	81.1	81.3	81.1	81.0	81.0
1.0	80.8	81.3	81.1	81.2	80.1

Impact of semantics decoupling on temporary concepts To understand which types of concepts most benefit from IPSeg, we categorize the 20 classes of Pascal VOC into 15 base classes and 5 new classes based on the incremental process. According to the learning objectives, all foreground classes are treated as temporary concepts in the corresponding step and the background is constantly considered as permanent ones. The comparison shown in Table 12 indicates that the new classes gain more significant performance improvement than the base classes. Furthermore, the permanent concepts (i.e.,

Table 11: (a): Ablation studies for hyper-parameters: memory size $|M|$, the ratio of noise filtering α_{NF} . (b): Ablation studies for hyper-parameters: the ratio of background compensation α_{BC} .

	value	0-15	16-20	all
$ M $	50	83.4	72.3	80.8
	100	83.5	75.1	81.5
	200	83.5	75.5	81.7
α_{NF}	0.2	83.5	75.0	81.4
	0.4	83.6	75.1	81.6
	0.6	83.4	74.6	81.3
	0.8	83.3	74.2	81.2
	1.0	83.4	74.7	81.3

(a)

α_{BC}	VOC 15-1 (6 steps)		
	0-15	16-20	all
1	82.9	74.9	81.0
0.9	83.5	75.1	81.6
0.8	83.5	75.0	81.5
0.7	83.4	74.4	81.3
0.6	83.3	74.3	81.2
0.5	83.2	73.8	81.0
0	80.6	66.6	77.3

(b)

the background) achieve less improvement compared to the temporary concepts. This observation suggests that IPSeg is more effective in enhancing the learning of new foreground classes.

Table 12: The ablation study of **SD** over background (BG), base foreground classes (Base) and new foreground classes (New) on Pascal VOC 15-1 with Swin-B backbone.

SD	BG	Base(1-15)	New(16-20)	All
\times	92.4	78.5	69.6	77.0
\checkmark	94.3(+1.9)	82.3(+3.7)	75.1(+5.5)	81.5

Detailed results of semantics decoupling on temporary concepts To understand which types of classes or concepts benefit from our method, we compare IPseg against the baseline on 20 classes of the VOC 15-1 setting. The detailed results are presented in Table 13, which demonstrates that IPSeg is more effective in enhancing the learning of new foreground classes.

Table 13: Detailed results of the ablation study for semantics decoupling (**SD**) over each class on Pascal VOC 15-1 with Swin-B backbone. Texts in red indicate 5 new classes.

SD	Detailed results											
\times	BG	plane	bike	bird	boat	bottle	bus	car	cat	chair	cow	
	92.4	87.4	37.7	89.1	67.8	80.4	93.8	86.9	93.6	43.9	85.7	
	tabel	dog	horse	motor	person	plant	sheep	sofa	train	TV	mIoU	
	63.8	90.0	87.2	85.9	84.1	57.5	81.6	53.3	87.1	68.4	77.0	
\checkmark	BG	plane	bike	bird	boat	bottle	bus	car	cat	chair	cow	
	94.3	91.8	43.8	93.8	75.0	86.0	94.2	91.2	96.1	44.3	94.6	
	tabel	dog	horse	motor	person	plant	sheep	sofa	train	TV	mIoU	
	67.3	94.5	93.0	88.8	88.2	65.6	90.1	57.9	89.3	72.7	81.5	

Class-wise results of IPSeg Table 14 shows the detailed experimental results of IPSeg for each class across four incremental scenarios of Pascal VOC 2012. IPSeg demonstrates superior performance in various incremental learning tasks, including standard tasks with a large number of initial classes (e.g., 15-5 and 15-1) and long-range tasks with fewer initial classes (e.g., 10-1 and 2-2). Notably, in the 2-2 task, the mIoU for “cow” and “horse” reaches 70.7% and 81.4%,

respectively. This indicates that IPSeg maintains excellent prediction performance even when classes with similar semantic information are trained in different stages.

Table 14: Class-wise results of IPSeg over each class.

VOC 15-5	BG	plane	bike	bird	boat	bottle	bus	car	cat	chair	cow
	93.6	92.2	44.9	93.8	74.4	85.2	93.9	90.8	96.2	43.0	94.5
	tabel	dog	horse	motor	person	plant	sheep	sofa	train	TV	mIoU
	68.0	94.2	92.9	88.0	88.0	66.3	91.5	46.4	87.8	74.4	80.9
VOC 15-1	BG	plane	bike	bird	boat	bottle	bus	car	cat	chair	cow
	94.3	91.8	43.8	93.8	75.0	86.0	94.2	91.2	96.1	44.4	93.5
	tabel	dog	horse	motor	person	plant	sheep	sofa	train	TV	mIoU
	67.4	94.5	92.9	88.8	88.2	66.4	88.6	58.1	89.5	72.7	81.5
VOC 10-1	BG	plane	bike	bird	boat	bottle	bus	car	cat	chair	cow
	93.1	93.1	42.2	93.2	72.1	83.5	93.9	91.9	95.8	38.0	86.9
	tabel	dog	horse	motor	person	plant	sheep	sofa	train	TV	mIoU
	54.1	91.8	86.1	87.5	87.5	64.2	85.6	49.9	88.4	72.1	78.6
VOC 2-2	BG	plane	bike	bird	boat	bottle	bus	car	cat	chair	cow
	91.4	88.6	39.3	87.9	71.5	71.9	89.1	78.2	89.3	28.8	70.7
	tabel	dog	horse	motor	person	plant	sheep	sofa	train	TV	mIoU
	55.2	83.5	84.1	77.6	82.6	63.6	72.1	44.4	82.1	69.1	72.4

Experimental results of disjoint setting To demonstrate IPSeg’s robust learning capability under different incremental learning settings and to further prove its superiority over general methods, we evaluate IPSeg using the disjoint setting on the Pascal VOC 2012 dataset for the 15-1 and 15-5 tasks, as shown in Table 15. The results indicate that IPSeg consistently achieves the best performance compared to state-of-the-art methods. Additionally, similar to the results in the overlap setting, IPSeg exhibits a strong ability to learn new classes while retaining knowledge of the old classes. Specifically, IPSeg outperformed the second-best method by **10.1%** in the 15-5 task and by **22.8%** in the 15-1 task in terms of new class performance.

Table 15: Comparison with state-of-the-art methods on Pascal VOC 2012 dataset for disjoint setup.

Method		VOC 15-5 (2 steps)			VOC 15-1 (6 steps)		
		0-15	16-20	all	0-15	16-20	all
Data-free	LwF-MC	67.2	41.2	60.7	4.5	7.0	5.2
	ILT	63.2	39.5	57.3	3.7	5.7	4.2
	MiB	71.8	43.3	64.7	46.2	12.9	37.9
	RCIL	75.0	42.8	67.3	66.1	18.2	54.7
Replay-based	SDR	74.6	44.1	67.3	59.4	14.3	48.7
	SSUL-M	76.5	48.6	69.8	76.5	43.4	68.6
	MicroSeg-M	80.7	55.2	74.7	80.0	47.6	72.3
	CoinSeg-M	82.9	61.7	77.9	82.0	49.6	74.3
	IPSeg(ours)	82.7	71.8	80.1	82.6	72.4	80.2

More qualitative results on Pascal VOC 2012 In addition to the qualitative results of the VOC 2-2 task shown in the main paper, we present additional qualitative analysis in Figure 8. We select the 15-1 task and perform a visual analysis for each newly added class. Each image includes both old and new classes, covering indoor and outdoor scenes as well as various objects and environments. For example, the first row shows the learning ability for ”plant”. After step 1, the model consistently predicts ”plant” correctly while retaining the ability to recognize ”dog”. Similarly, rows 2-5 show consistent performance. For each new class (i.e., sheep, sofa, train, and TV in the figure), IPSeg quickly adapts to them while retaining the ability to recognize old classes (i.e., bird, person, cat in the figure). These results clearly and intuitively demonstrate IPSeg’s strong capability in addressing incremental tasks.

More qualitative results on ADE20K The qualitative results of the 100-10 task on the ADE20K dataset are shown in Figure 9. We select five examples to illustrate the model’s ability to predict various classes as the learning step increases. Row 1 shows the performance of predicting the new class “ship” in step 1, where the model effectively recognizes both the old class “sky” and the new class “ship.” Similarly, in rows 2-5, for the newly introduced classes (tent, oven, screen, flag), IPSeg demonstrates excellent performance in learning the new classes without forgetting the old ones. This indicates that IPSeg achieves a balance between stability and plasticity even on more challenging and realistic datasets.



Figure 8: Qualitative results on Pascal VOC 2012 dataset with the 15-1 scenario.

IPSeg: Image Posterior Mitigates Semantic Drift in Class-Incremental Segmentation

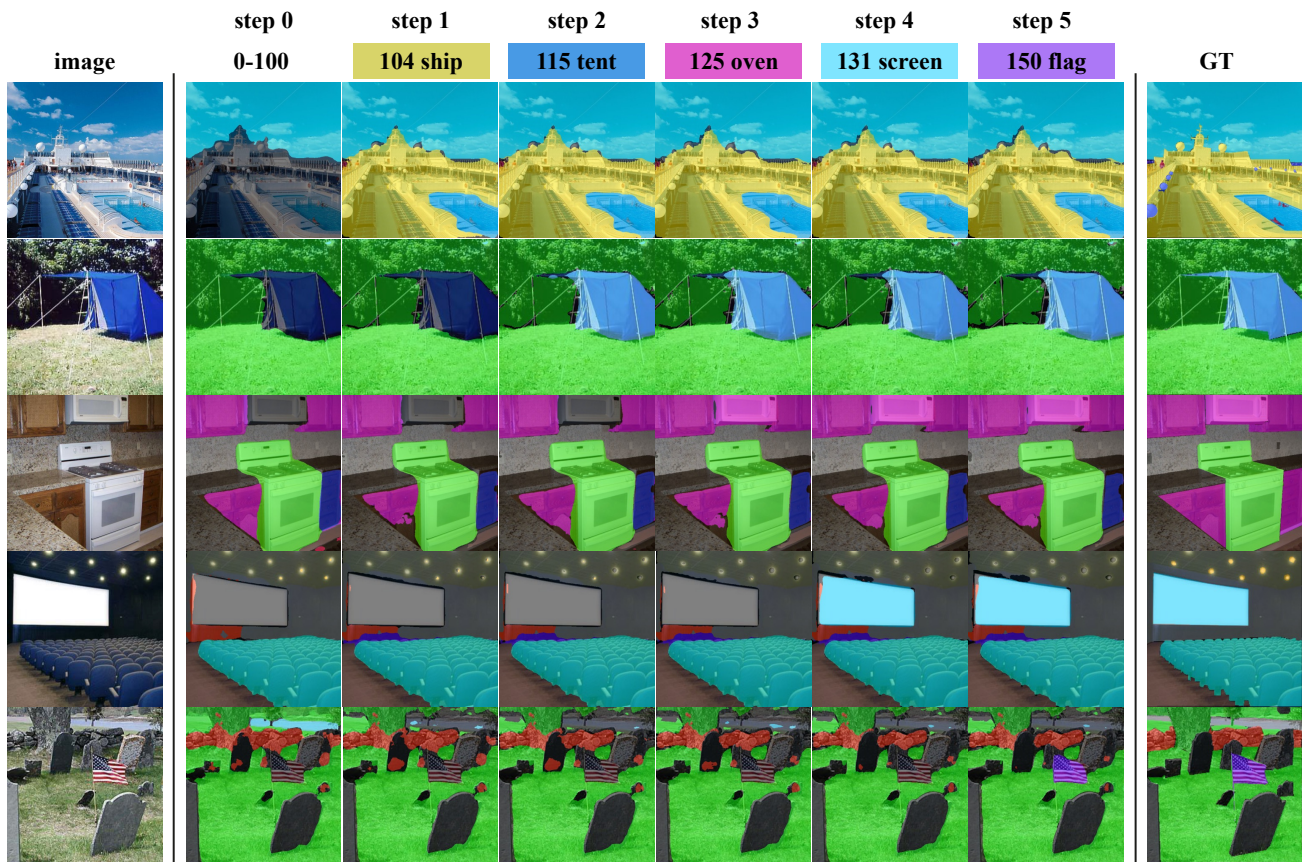


Figure 9: Qualitative results on ADE20K dataset with the 100-10 scenario.